Thin Solid Films 596 (2015) 101–110

Contents lists available at ScienceDirect

Thin Solid Films

journal homepage: www.elsevier.com/locate/tsf

The hybrid graphene multilayer system (graphene/SiN/graphene) coupled with titanium alloy (Ti6Al4V) — structural, mechanical and corrosion characterisation

M. Kalisz [a,*], M. Grobelny [a], M. Zdrojek [b], M. Świniarski [b], J. Judek [b]

[a] Motor Transport Institute, Centre for Material Testing, 80 Jagiellonska Street, Warsaw, Poland
[b] Faculty of Physics, Warsaw University of Technology, ul. Koszykowa 75, 00-662 Warsaw, Poland

ARTICLE INFO

Article history:
Received 30 March 2015
Received in revised form 24 July 2015
Accepted 24 July 2015
Available online 29 July 2015

Keywords:
Silicon nitride thin film
Nanoindentation
Electrochemical properties
Graphene
Graphene hybrid system

ABSTRACT

In this paper the studies on structural, mechanical and corrosion properties of the hybrid graphene multilayer system (graphene/SiN/graphene) coupled with titanium alloy (Ti6Al4V) have been investigated. We have shown that the graphene/SiN/graphene multilayer hybrid system deposited on titanium alloy surfaces, improves surface hardness (23 GPa) and the corrosion properties of the Ti6Al4V alloy in very aggressive environments. Furthermore, this multilayer hybrid system has a very stable course of electrochemical potential in comparison with pure silicon nitride thin film with the same thickness. Unfortunately, this system does not maintain structural and mechanical stability during the corrosion process. The structure of the coating system becomes porous, which is characterised by low hardness (0.62 GPa) and low Young's modulus — 69 GPa.

1. Introduction

Metallic biomaterials like Ti and Ti alloys are widely used for artificial hip joints, bone plates and dental implants owing to their excellent mechanical properties and endurance [1]. However, the long-term performance of surgical implants directly depends on their surface properties. Most implanted metallic biomaterials have a tendency to lose electrons in solution and, as a result, are very likely to corrode in the biological environments, which usually causes inflammation and a loosening of the implants [2]. Corrosion is the unwanted chemical reaction, which can result in a degradation of metal implants to oxides, hydroxides, and other compounds. These degradation products may cause a local inflammatory response, finally lead to the cessation of bone formation, synovitis, and a loosening of artificial joint implants [2]. Additionally, their low surface hardness, high friction coefficient and poor wear resistance also limit the application of metallic biomaterials [3,4]. The low wear resistance can lead to the formation of wear debris, causing several reactions in the tissue in which they are deposited, thus increasing the probability of the failure of the implants.

It is reported that wear and corrosion are the main reasons for the degradation of surgical implants such as hip and knee joint implants, which usually happens after 10–15 years of use [4]. To protect the metallic implants from corrosion and wear and improve their bioactivity, tremendous surface modification techniques have been applied to deposit a great variety of functional coatings on the surfaces of metallic implants.

There are two common ways to improve the corrosion and wear resistance of a metal implant. One is via bulk alloying and the other is via surface modification. Since this paper only focuses on the surfaces of metal implants, the first technology is not covered here.

One way to protect a titanium alloy surface from corrosion and improve its surface mechanical properties is the application of ceramic coatings *i.e.* silicon nitride.

This leads to the insulation of the metal from environmental stresses by the unbreakable, durable and elastic nitride films, which are at the same time wear resistant and harder than the titanium alloy surface [5]. Thin-film silicon nitride is characterised by its high density, low wear rate, good insulating properties, excellent Na^+ resistance, relatively high fracture toughness, strength, high temperature corrosion resistance in an oxidizing atmosphere and in a suiphidizing–oxidizing atmosphere [6] and excellent biocompatibility [7–10]. Silicon nitride films are an excellent diffusion barrier against water and aggressive contaminants which may corrode titanium alloys [11]. They can be deposited by low-pressure-chemical-vapour-deposition (LPCVD), plasma enhanced chemical vapour deposition (PECVD) or reactive radio frequency (r.f.) sputtering techniques. Unfortunately, their structural, mechanical and corrosion properties highly depend on the technological process used during the sample fabrication and processing [12–14].

* Corresponding author.

http://dx.doi.org/10.1016/j.tsf.2015.07.067
0040-6090/

The addition of a protective coating changes the dimensions of the metal due to the finite thickness of the coating. Changes also occur in the appearance and the optical properties of the metal surface. Furthermore, a decrease in the electrical and thermal conductivity can also be observed [13].

One important approach to overcome these problems would be to develop an ultrathin protective coating to minimise the variation in physical properties of the protected metal.

Graphene is a single atomic planar sheet of carbon, with a near perfect two-dimensional honeycomb crystal lattice. This material has many useful electrochemical characteristics, and with its high thermal conductivity, high inherent capacity and extremely large specific surface area, graphene outperforms many other materials. Numerous studies have demonstrated that graphene film, which features chemical inertness and thermal stability, is an excellent anticorrosion barrier for Cu [15–20] and other metals, such as Ti [21]. Unfortunately, a single layer of graphene does not change the mechanical properties of the surface on which is deposited [21].

It is reasonable to combine both types of coatings in a hybrid coating system having a thickness of several hundred nanometers and characterised by good mechanical properties and excellent corrosion resistance in aggressive environments, *e.g.* body fluids.

The purpose of this manuscript is to show that a hybrid coating system based on thin-film silicon nitride and graphene monolayers can be used as a layer system for the protection of a titanium alloy surface against the corrosion process and improve its surface mechanical properties. In this work, the surface, structural, mechanical and corrosion properties of a graphene/silicon nitride/graphene hybrid system has been investigated and compared with a pure titanium alloy and Ti–Al–V/SiN system.

2. Materials and methods

2.1. Experimental design

2.1.1. Specimen preparation

For the purpose of the experiment, two sets of titanium alloy Ti6Al4V samples (ASTM Grade 5, UNS R56400) (Table 1) were prepared in the same manner. Before the technological processes, the Ti alloy surfaces were polished using Stuers RotoPol 21 grinding and polishing apparatus. The sample surfaces were polished to a "mirror finish". In the next stage, the samples were cleaned in an acetone solution.

2.1.2. Preparation of the graphene monolayer

The graphene monolayers were grown on 18-μm thick copper foil using the chemical vapour deposition (CVD) technique. For this purpose a home-made CVD set based on the Blue M Tube Furnace with a 1-inch diameter reactor tube was used. During the growth process the reactor chamber is set to a low pressure ($\sim 10^{-6}$ Torr) and heated up to ~1000 °C in a hydrogen atmosphere. Methane is used as the carbon source (growth time is typically 10 min).

The graphene was transferred to the titanium alloy surface and the silicon nitride surface using the "PMMA-mediated" method [23]. First, the PMMA (495 K, about 100 nm thick) was spin-coated on top of the synthesised graphene on a copper substrate and then dried for 24 h at room temperature. Next the graphene from the bottom of the Cu substrate was etched using a reactive ion etching method in oxygen plasma (PlasmaLab 80+, Oxford Instruments). After that, the exposed Cu foil was dissolved in an aqueous etchant of iron (III) nitrate for several hours. When the copper dissolved the graphene sample was cleaned in DI (deionized) water. Next, the ion particles were removed using a hydrochloric acid solution — hydrogen peroxide as a catalyst dissolved in water [23]. After all the cleaning steps the PMMA/graphene layer was transferred to the surfaces and annealed in order to evaporate the water and increase adhesion between the graphene and the surface. In the last step, the PMMA layer was removed.

Table 1
Composition of Ti6Al4V titanium alloy.

Components, wt. %						
C	Fe	N	O	Al	V	Ti
0.08	0.25	0.05	0.20	5.50–6.75	3.5–4.5	Bal

Table 2
Summary of the Si_xN_y process parameters.

RF power [W]	120
Pressure [Torr]	0.8
SiH_4 gas flow [ml/min]	150
NH_3 gas flow [ml/min]	50
Temperature [°C]	350

2.1.3. Preparation of the thin-film silicon nitride

The amorphous films of silicon nitride were fabricated in an Oxford Plasma Technology PlasmaLab 80 Plus System, which is a parallel plate PECVD (13.56 MHz) deposition system. The system allows users to predefine the process parameter value and control it in real-time during the process. Films prepared using the PECVD method have a lot of advantages, such as low deposition temperature, high growth rate, good uniformity and good adhesion to the substrate surface [22].

Table 2 shows a summary of the parameters used for the deposition of SiN film in this study.

2.1.4. Preparation of the test samples

Figure 1 shows schematically the procedure for the test samples preparation.

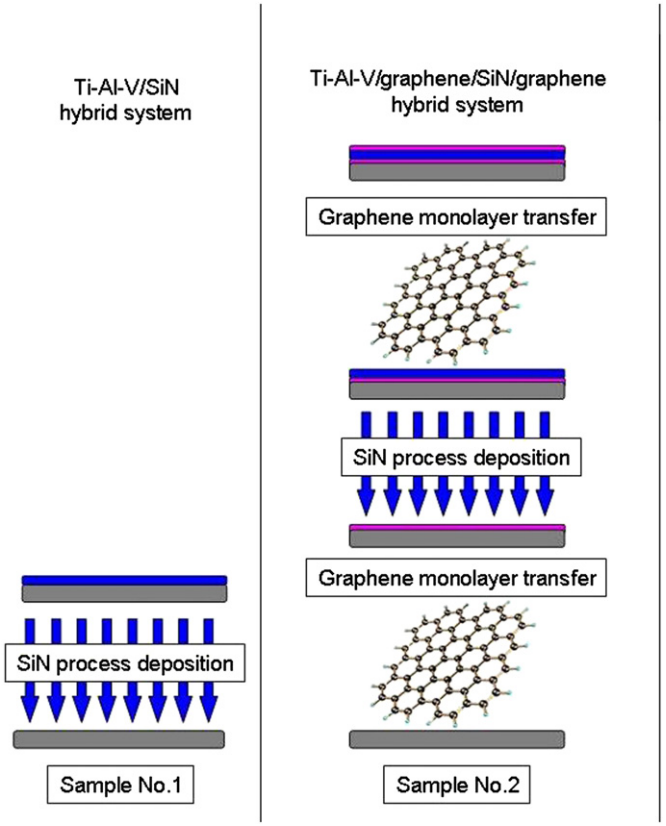

Fig. 1. Schematics showing the preparation of the test samples.

2.2. Analysis of surface characteristics

The quality and the number of transferred layers of graphene were evaluated by Raman spectroscopy (InVia Renishaw Spectrometer, 514 nm laser line, standard mode). All Raman spectra were collected at room temperature using 1 mW of laser power (on the sample).

Raman spectroscopy is a non-destructive and fast method for studying, e.g. various carbon materials. In the case of graphene, Raman spectra provide information on the number of layers [24], material quality and defects [25]. Typical Raman spectra consist of three main modes: D mode (~1350 cm^{-1}), G mode (~1580 cm^{-1}) and 2D mode (~2700 cm^{-1}). A monolayer graphene sheet is easily identified by a Raman study simply by looking at the G/2D relative intensity ratio (usually about 0.2), also taking into account the shape of those peaks [24]. The quality and defectiveness of a graphene sheet can be verified by the appearance of a D mode peak, usually taken as the relative ID/IG ratio [26,27].

The thickness of the thin films of silicon nitride deposited was measured by a Taylor Hobson Talysurf CCI Lite optical profilometer, and was 200 nm.

The elemental composition and the surface morphology of the deposited coating system were investigated with the aid of a Zeiss FE-SEM Merlin with EDS Quantax System (Bruker) and Raith e-Line Plus (FE Zeiss column, 30 keV) scanning electron microscope.

To determine the surface topography, atomic force microscopy (AFM) measurements were made using the MultiMode 8 AFM microscope (Bruker) with Peak Force Tapping mode.

Raman spectroscopy measurements, SEM measurements and AFM measurements were performed after each step of the technological process, during test sample preparation.

2.3. Mechanical characterisation

The hardness and Young's modulus measurements of the coating systems, obtained before and after the corrosion process, were performed by a nanoindenter manufactured by CSM Instruments (Switzerland) equipped with a diamond Vickers indenter. Both parameters were calculated using the method proposed by Oliver and Pharr [28]. Each data point represents an average of five indentations. A number of measurements were carried out for various depths of nanoindentation (from 80 nm to 700 nm). In order to measure the "film-only" properties and minimise the impact of the substrate, a method of approximating the nanoindentation measurements was implemented [29].

The hardness was expressed as functions $H(H_f,H_s,h/d)$, with subscripts f and s denoting film and substrate. Then a simple approach previously used by Hu in [30] for spherical indentations, by writing hardness H as a power-law function:

$$H = H_s \times \left(H_f/H_s\right)^M \tag{1}$$

where the exponent terms are a dimensionless spatial function

$$M = M(h/d) \tag{2}$$

was used (h — indentation depth, d — film thickness). This formulation conveniently separates material and geometry terms.

Eq. (1) must satisfy essential boundary conditions:

$h/d \to 0$, $H = H_f$, $L = 1$ and $M = 1$ (small penetrations, film-dominated limit) and $h/d \to \infty$, $H = H_s$, $L = 0$ and $M = 0$ (large penetrations, substrate-dominated limit).

These boundary conditions are most simply and smoothly satisfied by sigmoidal functions:

$$L = 1/[1 + A(h/d)^C \tag{3}$$

$$M = 1/[1 + B(h/d)^D \tag{4}$$

where A, B, C, and D are adjustable coefficients.

2.4. Electrochemical measurements

Electrochemical measurements were carried out in 0.5 M/l NaCl, 2 g/l KF, pH = 2 adjusted by concentrated hydrochloric acid. The solution (0.5 M NaCl, pH 2, 2 g/l KF) in which the electrochemical measurements were taken is characterised by a high corrosivity compared to titanium alloys. It is a more aggressive environment than that of typical electrolytes for corrosion tests (e.g. artificial saliva, SBF) [31–36]. Voltammetric measurements (polarisation curves) were carried out at a scan rate of 1 mV/s within a range of −150 mV to 1000 mV versus open circuit potentials, and polarisation curves corresponding to all examined material were recorded. Prior to each polarisation experiment, the samples were immersed in the electrolyte for 1 h while monitoring open circuit potential to establish steady state conditions. Each electrochemical measurement for the same material, was performed for three times. In the paper we show only the most representative results. However, the differences between the successive values of the open circuit potential (for the same material) did not exceed 50 mV. A three-electrode cell arrangement was applied using the Ag/AgCl electrode with a Luggin capillary as reference electrode and a platinum wire as the auxiliary electrode (counter electrode). The measurements were carried out by means of an Autolab EcoChemie System of the AUTOLAB PGSTAT 302N type equipped with GPESv. 4.9. software in aerated solutions at room temperature. The values of corrosion current densities (i_{corr}) were obtained from the polarisation curves by extrapolating the cathodic and anodic branch of the polarisation curves to the corrosion potential [37].

3. Results and discussion

3.1. Structural characterisation of TiAlV/graphene/SiN/graphene coatings system before corrosion process

In Fig. 2, an AFM image of the titanium alloy surface covered by the graphene monolayer is shown. The graphene layer is smooth, without cracks or damage, which is confirmed by the Raman measurements.

In the Raman spectra for graphene layer deposited on the titanium alloy surface (Fig. 3a), the negligible D mode is seen, suggesting that

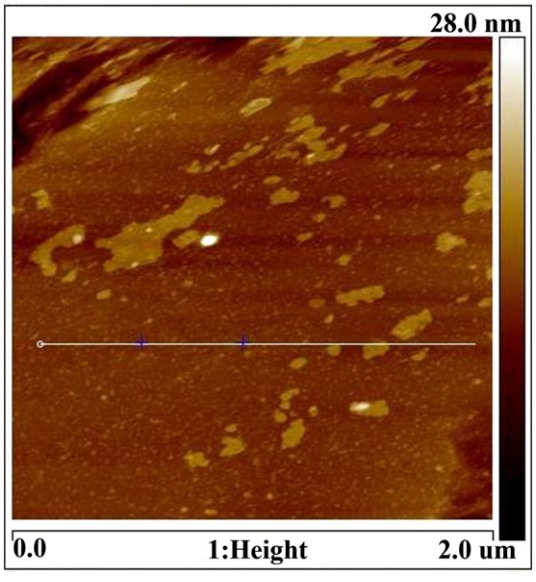

Fig. 2. AFM image of titanium alloy covered by the graphene monolayer.

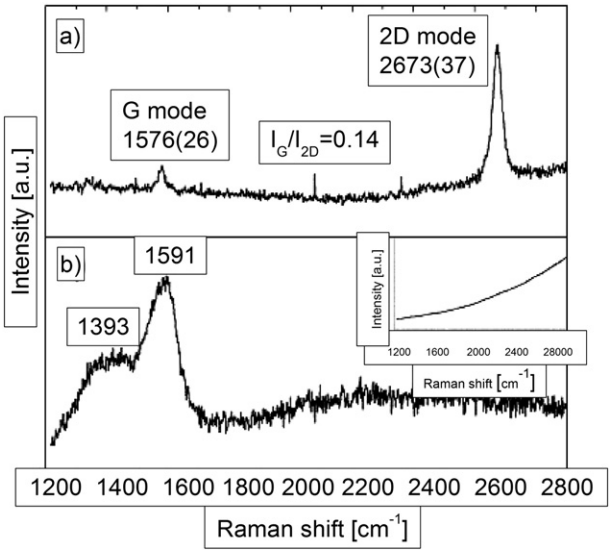

Fig. 3. Raman spectrum of graphene monolayer a) deposited on top of titanium alloy surface; b) taken in the SiN peeled off area showing significantly damaged carbon layer. Inset: spectrum collected in the place where SiN is not peeled off.

the graphene layer is without structural defects. Furthermore the intensity ratio of the G and 2D modes shows that this is indeed monolayer graphene.

After the SiN deposition we found some areas where the SiN layer had peeled off from the graphene surface, forming holes in the SiN layer, which suggests low silicon nitride adhesion to the thin carbon layer (see Fig. 4).

The Raman spectra collected in the peeled-off areas show the existence of amorphous carbon (Fig. 3b) [44]. So, it appears that the SiN deposition process seems to strongly deteriorate the quality of deposited graphene. The inset in Fig. 3b corresponds to the signal collected on the SiN layer that was supposed to cover the graphene layer, but this time showing no evidence of carbon. This might be caused by the fact that SiN completely screens the Raman signal of carbon from the underling layer, especially if this is an amorphous carbon layer, which would normally have a lower intensity than graphene.

In the SEM image (Figs. 5) obtained after the last stage of the technological process — deposition of the graphene layer on the top of the SiN thin film surface — not only are the grains of the graphene layer seen, but also cracks and flaking thin-film silicon nitride located under it.

In the Raman spectra for graphene, an increase in the D mode is seen, suggesting that the graphene layer has structural defects. These defects

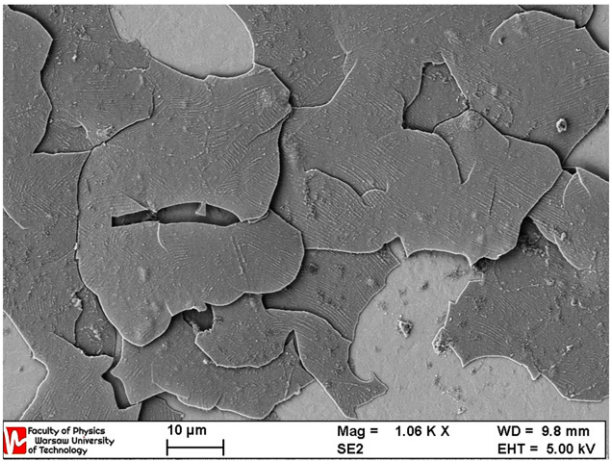

Fig. 4. The thin-film silicon nitride deposited on the titanium alloy surface covered with the graphene monolayer.

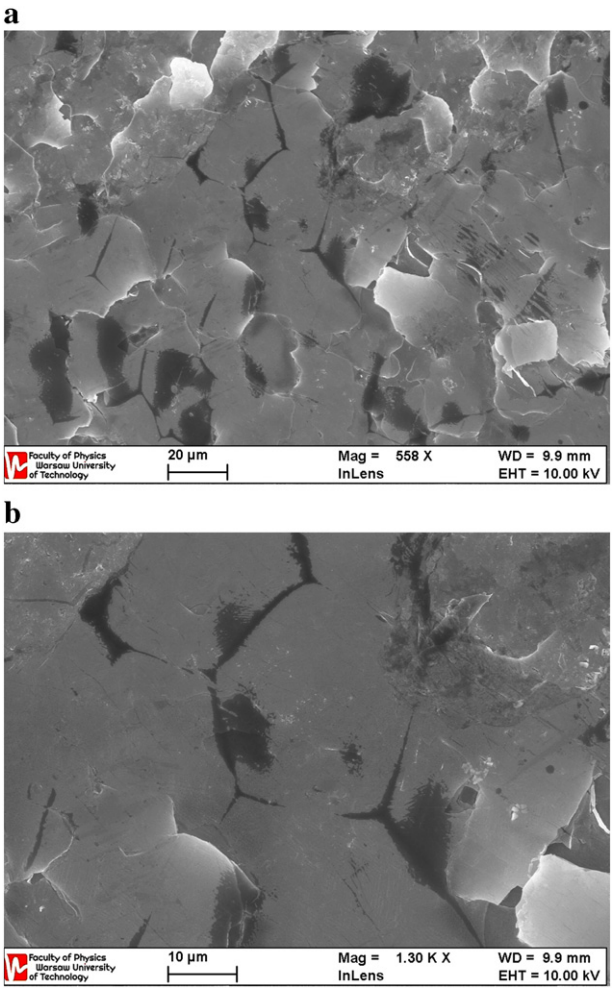

Fig. 5. SEM pictures of sample with graphene deposited on top of grain structure of SiN layer and with cracks. B zoom in the centre area seen in A.

could have been caused by the cracks and damage to the thin-film silicon nitride located under the graphene layer. Furthermore, the intensity of the main modes might suggest worse graphene layer adhesion to the SiN surface. Unfortunately, based on the intensity ratio of the G and 2D modes, it is not possible to conclude that we observe a monolayer of graphene on top of the coating system formed (Fig. 6).

For comparison, the pure thin-film silicon nitride on the titanium alloy surface, was deposited. The SEM observation of the sample shows that the thin-film silicon nitride was crack free, exhibited good adherence to the substrate, no discontinuation of the thin film was observed and the surface morphology was homogeneous (see Fig. 7).

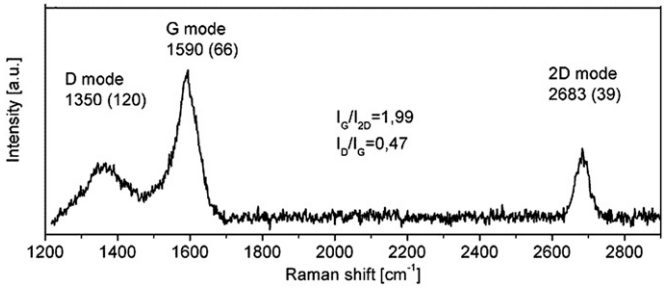

Fig. 6. Raman spectrum of graphene monolayer deposited on top of the silicon nitride thin film (last step of graphene/SiN/graphene hybrid system process preparation).

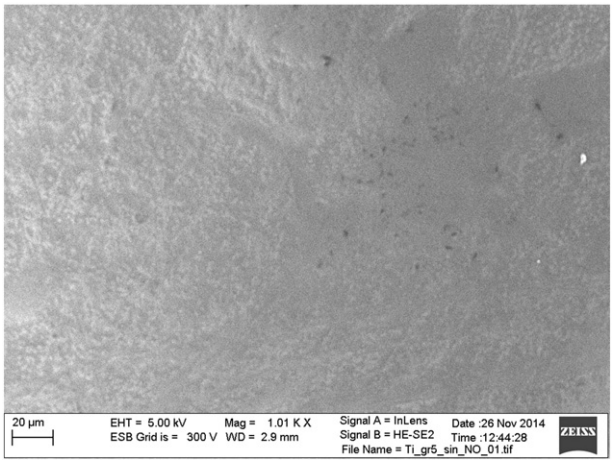

Fig. 7. The thin-film silicon nitride deposited on the uncoated titanium alloy surface.

3.2. Potentiodynamic tests

Figs. 8a and b shows the course of the open cell potential (OCP) and the course of the polarisation curves of titanium alloy and titanium alloys with the tested coating system in 0.5 M/l NaCl, 2 g/l KF, pH = 2 electrolyte solution. The results of the measurements of the electrochemical parameters of the samples obtained from the polarisation curves are collected in Table 3.

Table 3
Corrosion test results of Ti6Al4V alloy and Ti6Al4V alloy with tested coatings system obtained from polarisation curves in 0.5 M NaCl, pH = 2, 2 g/l KF solution.

Sample	i_{corr} [A/cm^2]	E_{corr} [V]
TiAlV/graphene/SiN/graphene	3.3E − 08	0.176
TiAlV/SiN	5.8E − 08	−0.866
Ti6Al4V	6.1E − 05	−1.188

After depositing the graphene/SiN/graphene coating system on the titanium alloy surface a significant improvement in the corrosion properties is seen, expressed by a decrease of corrosion current density (i_{corr}) and a shift in corrosion potential (E_{corr}) values to the noble potentials. The smallest corrosion current density and the best corrosion properties were obtained for the TiAlV/graphene/SiN/graphene coating system. The smaller the value of the corrosion current density, the better corrosion properties a tested coating system exhibits. For this sample, the most positive value of corrosion potential was also obtained (E_{corr} = 0.176 V). A positive corrosion potential value is characteristic for materials with low electrochemical activity and thereby shows very good corrosion resistance. It should also be noted that the course of the potential is very stable. During 1 h of exposure the potential changed only by about 110 mV. For the uncoated titanium alloy sample after about 2400 s a sharp decline in the value of the potential from −0.75 V to −1.20 V takes place. This change is caused by damage to the oxide layer present on the surface of the titanium alloy. The oxide layer acts as a barrier and protects against general corrosion processes. However, in the acidic pH environment (pH ca. 2) the protective layer

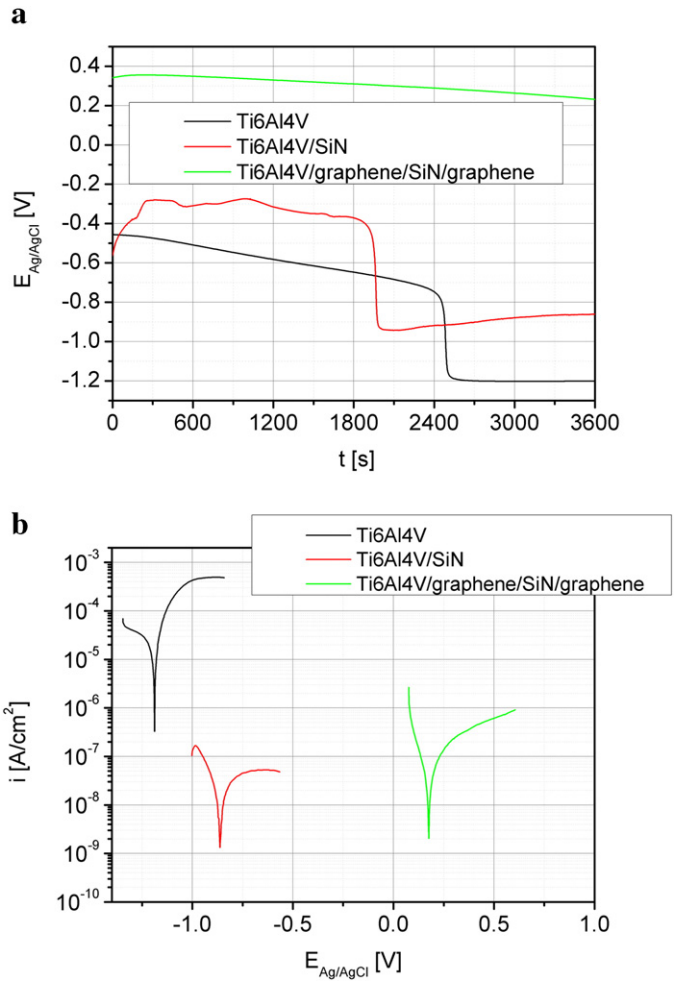

Fig. 8. Open circuit potential (OCP) (a) and polarisation curves (b) of Ti6Al4V titanium alloy and titanium alloy with coating system.

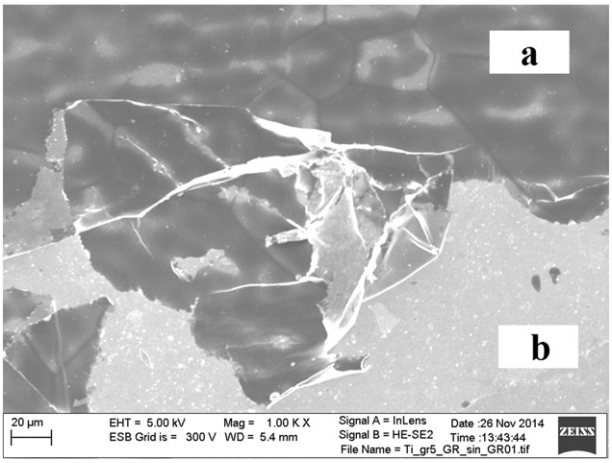

Fig. 9. SEM image of the graphene/SiN/graphene coatings system after corrosion process.

is unstable and the corrosion processes of the metallic Ti or its alloys are initiated. This phenomenon is accelerated in the presence of aggressive ions such as fluoride ions [38–41]. A similar course of OCP for titanium alloy covered by the thin-film SiN was observed. In this case after about 1800 s a sharp decline in the value of the potential from −0.4 V to −0.9 V takes place. This is probably due to the penetration of the coating by the electrolyte, which starts the corrosive reaction of the titanium alloy.

3.3. Structural characterisation of the TiAlV/graphene/SiN/graphene coating system after the corrosion process

Fig. 9 shows that after the corrosion process, in the corroded area two completely different regions were formed: continuous and porous. It seems, that the corrosion process produces a continuous thin film of silicon nitride in the porous layer, under which the edges of the graphene layer grains are clearly visible.

The results of the x-ray microanalysis showed that both regions consist of the same components, i.e. silicon and nitride (which are the components of the deposited thin-film silicon nitride), carbon and oxide (Fig. 10a–b). However, depending on the measured region, a change in the carbon content is observed. For the porous region the carbon content is higher, which is probably caused by exposing the graphene monolayer located at the structure interface. The amount of nitrogen, oxygen and silicon, in both cases, is almost constant.

Fig. 11 shows the morphology of the continuous region of thin-film silicon nitride viewed at a magnification of 49 k. As can be seen, the surface of the thin-film silicon nitride is not smooth and looks like "orange peel" (see Fig. 11) [42].

The porous region is clearly visible in Fig. 12a taken at a magnification of 111 k. Interestingly, the porous layer is not as fragile as the originally deposited thin-film silicon nitride but flexible, see Fig. 12b.

For further information about the surface topography of the graphene/SiN/graphene coating system after the corrosion process, AFM measurements were performed. In Fig. 13 the AFM images for the continuous (Fig. 13b) and porous (Fig. 13a) regions of the graphene/silicon nitride/graphene coating system are shown. Fig. 13b

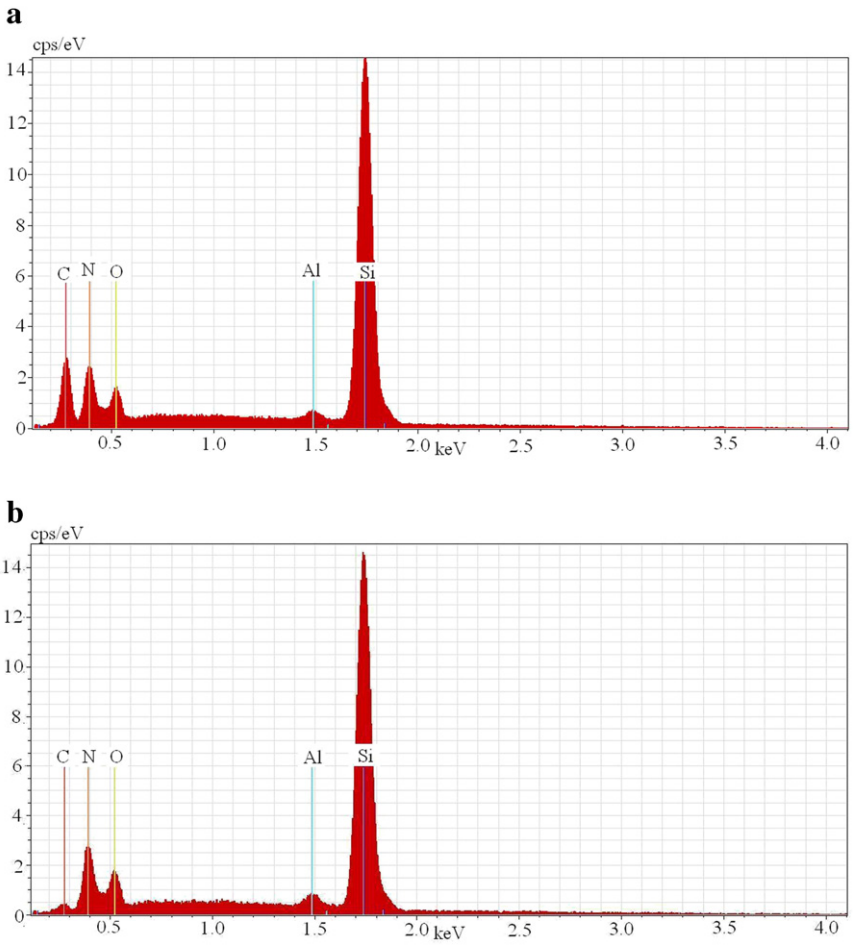

Fig. 10. Results of x-ray microanalysis showing the chemical composition of the: a) porous area, b) continuous area, both after corrosion process.

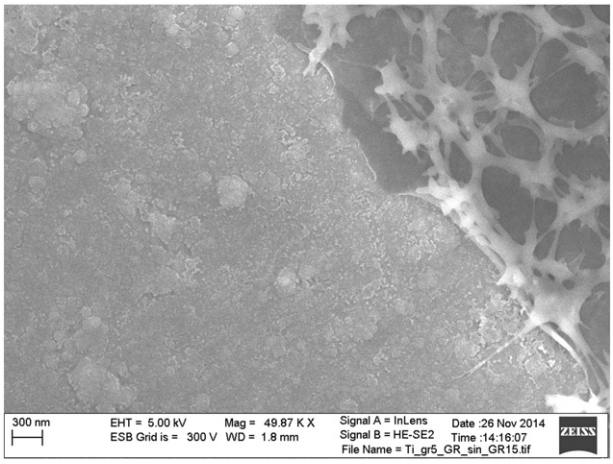

Fig. 11. SEM image of continuous region of graphene/SiN/graphene hybrid system formed after corrosion process.

suggesting that after the corrosion process, the thin film remaining on the surface is densely packed. Most of the boundaries between two adjacent grains in the silicon nitride from the graphene/silicon nitride/graphene coating system, are "sealed" [43]. It looks like the top layer of the graphene/SiN/graphene coating system is composed of many big particles, quite regular in shape, and with a height of about 85 nm. During the SEM measurements these particles may resemble the "orange peel" (see Fig. 11).

For the porous region, in the AFM image the holes and empty spaces are clearly visible. The depth of these holes is at about 200 nm (the thickness of the originally deposited thin-film silicon nitride) (Fig. 13a).

Fig. 14 shows the Raman spectra collected after corrosion process of the Ti–Al–V/grapheneSiN/graphene coating system. The decrease of the intensity of the main modes after the corrosion process might suggest good graphene layer adhesion to the surface. The relative intensity ratios after corrosion indicating that the defective graphene layer has not changed. The shift of the positions of the peaks might suggest a change in the doping level of the graphene, and the removal of some amount of chemical leftover. The higher purity of the graphene layer is caused by the corrosion solution process, where most of the contaminants that are left after the chemical transfer process (e.g. the Fe^{+3} ions that are left after the copper etching process, PMMA residues) are washed out.

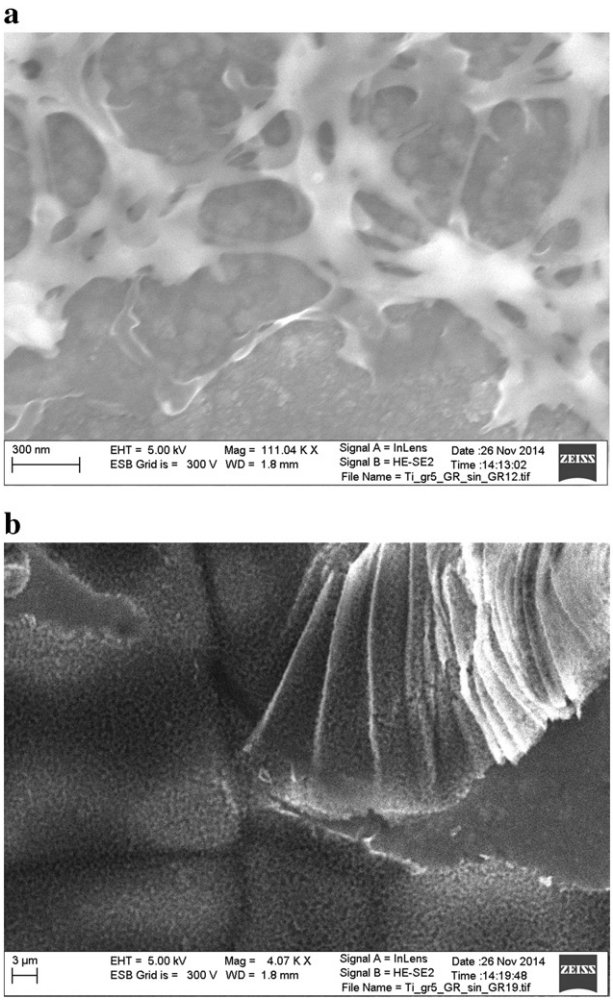

Fig. 12. SEM image of: a) porous region of graphene/SiN/graphene hybrid system formed after corrosion process, b) the flexible part of porous region of graphene/SiN/graphene hybrid system.

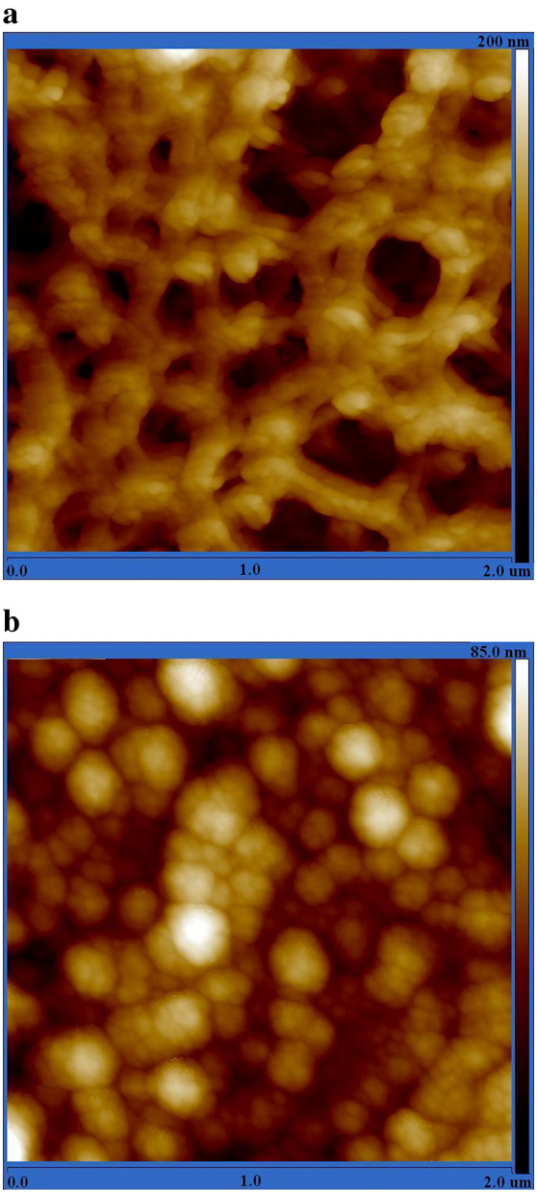

Fig. 13. AFM images of a) porous region, b) continuous region of graphene/SiN/graphene hybrid system formed after corrosion process.

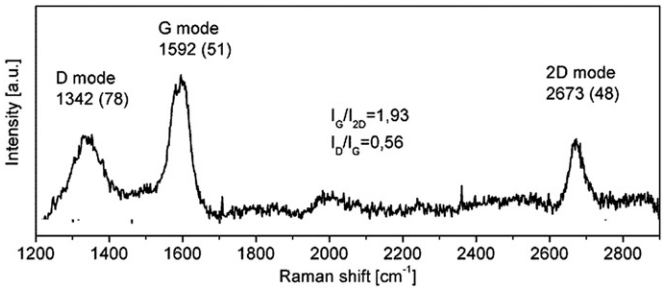

Fig. 14. Raman spectra of the Ti–Al–V/grapheneSiN/graphene layered structure collected after corrosion process.

For comparison, the thin-film silicon nitride after the corrosion process, exhibits clearly visible holes (Fig. 15). This is probably due to the penetration of the coating by the electrolyte, whereby the SiN layer is degraded.

As can be seen, in both cases, during the corrosion process the SiN layer is degraded. However, in the case of a graphene/SiN/graphene hybrid coating system, the degradation of the SiN layer is probably compensated by the presence of graphene monolayers, providing the high corrosion resistance of the coating system formed.

3.4. Mechanical characterisation of TiAlV/graphene/SiN/graphene coating system before and after the corrosion process

The hardness and Young modulus of the prepared coating system were measured using the nanoindentation technique and determined by an approximation method. For pure titanium alloy, nanohardness was measured at a constant depth of 80 nm. This is the smallest depth for which correct results have been obtained. Additionally, the root mean square error (RMSE) was calculated.

The surface hardness obtained for the uncoated titanium alloy, titanium alloy covered by the thin-film silicon nitride and titanium alloy covered with the graphene/silicon nitride/graphene coating system, was equal to 5.94 GPa ± 0.4 GPa, 22.4 GPa ± 1.0 GPa (Fig. 16b) and 23.0 GPa ± 1.0 GPa (Fig. 16a), respectively. Compared to the results presented in the literature reports, the hardness of the thin-film silicon nitride in question is higher by approx. 51% [45–48] and 22% [48].

The Young's modulus obtained for uncoated titanium alloy, titanium alloy covered with the thin-film silicon nitride and graphene/silicon nitride/graphene coating system, was equal to 107 GPa ± 3.2 GPa, 232 GPa ± 0.6 GPa (Fig. 17b) and 234 GPa ± 0.5 GPa (Fig. 17a), respectively. Schneider and Tucker reported a Young's modulus of 230–265 GPa for 0.2–0.3 μm thin-film silicon nitride [49], and Tabata et. al. obtained 290 GPa for 0.5 μm thin-film silicon nitride [50].

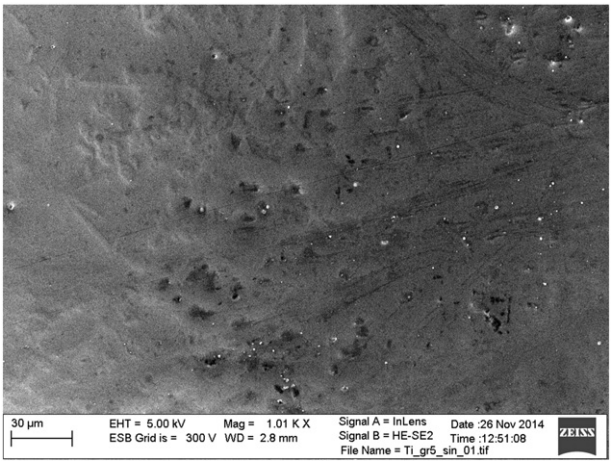

Fig. 15. SEM image of SiN thin film deposited on titanium alloy surface after corrosion process.

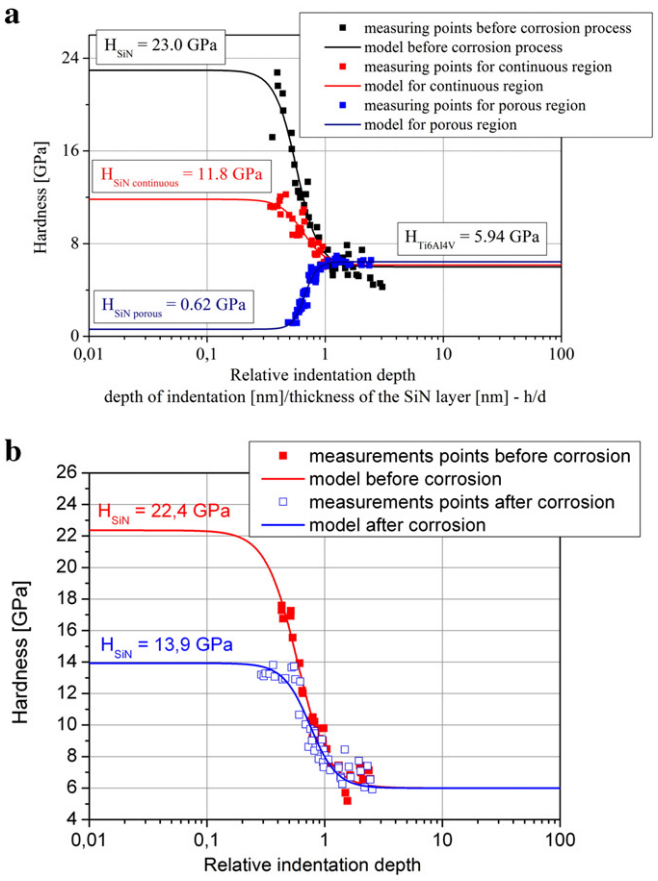

Fig. 16. Results of hardness investigation for a) graphene/SiN/graphene hybrid system and b) SiN thin film, before and after corrosion process.

As can be seen, the graphene monolayer deposited on top of the thin-film silicon nitride and embedded between the titanium alloy surface and the thin-film silicon nitride, is practically not seen by the nanoindenter during measurements. Therefore, the measurement did not reveal changes in the value of the hardness and the Young's modulus of the thin-film silicon nitride after the introduction of this layer between two graphene monolayers, in comparison with pure thin-film silicon nitride.

Nanoindentation measurements, performed after the corrosion process, show a decrease of both the hardness and the Young's modulus, of the silicon nitride and the graphene/silicon nitride/graphene coating systems.

The hardness obtained for the pure thin-film silicon nitride after the corrosion process was equal to 13.9 GPa ± 0.7 GPa (Fig. 16b). For the graphene/silicon nitride/graphene coating system, the hardness after the corrosion process was dependent on the structure of the region measured, and was equal to: for the continuous and porous regions: 11.8 GPa ± 0.7 GPa and 0.62 GPa ± 0.05 GPa, respectively (Fig. 16a).

The value of the Young's modulus obtained for the titanium alloy covered with the thin-film silicon nitride was equal to 164 GPa ± 13 GPa (Fig. 17b). In the case of the sample coated with the graphene/silicon nitride/graphene coating system, the Young's modulus for the continuous regions was equal to 143 GPa ± 6 GPa and for the porous region: 64 GPa ± 2.6 GPa (Fig. 17a). It is clear that the corrosion process causes the oxidation of the thin-film silicon nitride in both samples tested, and the formation of Si–O bonds. The existence of Si–O bonds embedded in the thin-film silicon nitride tends to lower the hardness and elasticity moduli down to values similar to the silicon oxide [50].

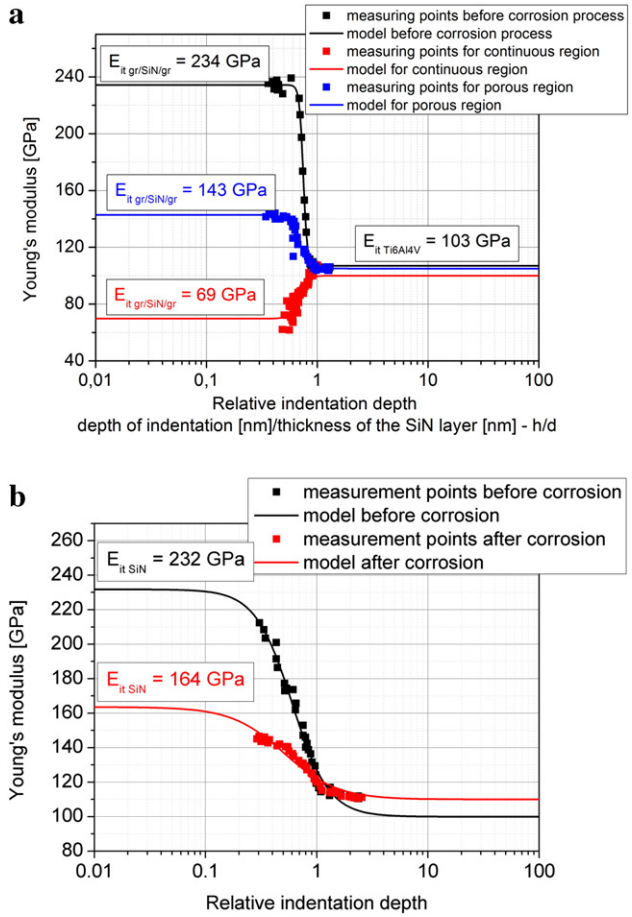

Fig. 17. Results of Young's modulus investigation for a) graphene/SiN/graphene hybrid system and b) SiN thin film, before and after corrosion process.

4. Summary

We have shown that the graphene/SiN/graphene coating system deposited on titanium alloy surfaces can be considered a coating system that improves the surface hardness and corrosion properties of the Ti6Al4V alloy. The graphene/SiN/graphene hybrid system protects the titanium alloy surface against corrosion processes which take place on pure titanium alloy surfaces in very aggressive environments. Furthermore, this coating system has a very stable course of electrical potential in comparison with pure thin-film silicon nitride of the same thickness.

Unfortunately, this system does not maintain structural and mechanical stability during the corrosion process. The structure of the coating system becomes porous, which is characterised by low hardness and high elasticity (low Young's modulus). In addition, the SiN layer is characterised by low adhesion to the substrate coated with a graphene monolayer. The thin-film silicon nitride breaks and comes away from the surface during the process of the creation of the hybrid system.

In the next step, investigations into the durability of the corrosion and mechanical properties of hybrid systems during temporary exposure in corrosive environments (artificial saliva, SBF etc.) will be performed.

Acknowledgements

This work was financed by the National Centre for Research and Development in 2013–2016 as research project no. GRAF-TECH/NCBR/14/26/2013 "InGrafTi".

References

[1] M. Niinomi, Metallic biomaterials, J. Artif. Organs 11 (2008) 105–110.
[2] S.P. Patterson, R.H. Daffner, R.A. Gallo, Electrochemical corrosion of metal implants, AJR Am. J. Roentgenol. 184 (2005) 1219–1222.
[3] E. Ingham, J. Fisher, Biological reaction to wear debris in total joint replacement, Proc. Inst. Mech. Eng. H. 214 (2000) 21–37.
[4] M. Spector, Biomaterial failure, Orthop. Clin. North Am. 23 (1992) 211–217.
[5] X. Liua, P.K. Chub, Ch. Dinga, Surface modification of titanium, titanium alloys, and related materials for biomedical applications, Mater. Sci. Eng. R 47 (2004) 49–121.
[6] J. Pitter, J. Cizner, F. Černý, M.A. Djouadi, A. Koutsomichalis, The influence of gradient SiN*x* IBAD coating on corrosion resistance of alloy steels in oxidizing and sulphidizing—oxidizing atmospheres at high temperature, Surf. Coat. Technol. 90 (1998) 1169–1173.
[7] M. Mazzocchi, A. Bellosi, On the possibility of silicon nitride as a ceramic for structural orthopedic implants. Part I: processing, microstructure, mechanical properties, cytotoxicity, J. Mater. Sci. Med. 19 (8) (2008) 2881–2887.
[8] M. Mazzocchi, D. Gardini, P. Luigi Traverso, M. Giulia Faga, A. Bellosi, On the possibility of silicon nitride as a ceramic for structural orthopaedic implants. Part II: chemical stability and wear resistance in body environment, J. Mater. Sci. Med. 19 (8) (2008) 2889–2901.
[9] S.B. Bal, A. Khandkar, R. Lakshminarayanan, I. Clarke, A.A. Hoffman, M.N. Rahaman, Testing of silicon nitride ceramic bearings for total hip arthroplasty, J. Biomed. Mater. Res. B Appl. Biomater. 87B (2) (2008) 447–454.
[10] S.B. Bal, A. Khandkar, R. Lakshminarayanan, I. Clarke, A.A. Hoffman, M.N. Rahaman, Fabrication and testing of silicon nitride bearings in total hip arthroplasty: winner of the 2007 "HAP" PAUL Award, J. Arthroplast. 24 (1) (2009) 110–116.
[11] M.-Ch. Joa, S.-K. Park, S.-J. Park, A study on the resistance of PECVD silicon nitride thin film to thermal stress-induced cracking, Appl. Surf. Sci. 140 (1999) 12–18.
[12] J. Olofsson, T. Mikael Grehk, T. Berlind, C. Persson, S. Jacobson, H. Engqvist, Evaluation of silicon nitride as a wear resistant and resorbable alternative for total hip joint replacement, Biomater 2 (2) (2012) 94–102.
[13] Z. Shi, Y. Wang, C. Du, N. Huang, L. Wang, C. Ning, The structure, surface topography and mechanical properties of Si–C–N films fabricated by RF and DC magnetron sputtering, Appl. Surf. Sci. 258 (4) (2011) 1328–1336.
[14] Z. Shi, Y. Wang, C. Du, N. Huang, L. Wang, C. Ning, Silicon nitride films for the protective functional coating: blood compatibility and biomechanical property study, J. Mech, Behav. Biomed. Mater. 16 (2012) 9–12.
[15] R.K.S. Raman, P.C. Banerjee, D.E. Lobo, H. Gullapalli, M. Sumandasa, A. Kumar, L. Choudhary, R. Tkacz, P.M. Ajayan, M. Majumder, Protecting Cu from electrochemical degradation by graphene coating, Carbon 50 (2012) 4040–4045.
[16] G. Kalita, M.E. Ayhan, S. Sharma, S.M. Shinde, D. Ghimire, K. Wakita, M. Umeno, M. Tanemura, Low temperature deposited graphene by surface wave plasma CVD as effective oxidation resistive barrier, Corros. Sci. 78 (2014) 183–187.
[17] A.S. Kousalya, A. Kumar, R. Paul, D. Zemlyanov, T.S. Fisher, Graphene: an effective oxidation barrier coating for liquid and two-phase cooling systems, Corros. Sci. 69 (2013) 5–10.
[18] N.T. Kirkland, T. Schiller, N. Medhekar, N. Birbilis, Exploring graphene as a corrosion protection barrier, Corros. Sci. 56 (2012) 1–4.
[19] S.S. Chen, L. Brown, M. Levendorf, W.W. Cai, S.Y. Ju, J. Edgeworth, X.S. Li, C.W. Magnuson, A. Velamakanni, R.D. Piner, J.Y. Kang, J. Park, R.S. Ruoff, Oxidation resistance of graphene-coated Cu and Cu/Ni alloy, ACS Nano 5 (2011) 1321–1327.
[20] D. Prasai, J.C. Tuberquia, R.R. Harl, G.K. Jennings, K.I. Bolotin, Graphene: corrosion-inhibiting coating, ACS Nano 6 (2012) 1102–1108.
[21] M. Kalisz, M. Grobelny, M. Mazur, D. Wojcieszak, M. Świniarski, M. Zdrojek, J. Domaradzki, D. Kaczmarek., Mechanical and electrochemical properties of Nb2O5, Nb2O5:Cu and graphene layers deposited on titanium alloy (Ti6Al4V), Surf. Coat. Technol. 271 (2015) 92–99.
[22] L. Liu, W.-G. Liu, N. Cao, Ch-L. Cai., Study on the performance of PECVD silicon nitride thin films, Def. Technol. 9 (2013) 121–126.
[23] X. Liang, B.A. Sperling, I. Calizo, G. Cheng, C.A. Hacker, Q. Zhang, Y. Obeng, K. Yan, H. Peng, Q. Li, X. Zhu, H. Yuan, A.R. Hight Walker, Z. Liu, L. Peng, C.A. Richter, Toward clean and crackless transfer of graphene, ACS Nano 5 (2011) 9144–9153.
[24] A. Jorio, R. Saito, G. Dresselhaus, M.S. Dresselhaus, Raman Spectroscopy in Graphene-Based Systems: Prototypes for Nanoscience and Nanometrology, Wiley-VCH, 2011.
[25] V. Singh, D. Joung, L. Zhai, S. Das, S.I. Khondaker, S. Seal, Graphene based materials: past, present and future, Prog. Mater. Sci. 56 (2011) 1178–1271.
[26] A. Gupta, G. Chen, P. Joshi, S. Tadigadapa, P.C. Eklund, Raman scattering from high-frequency phonons in supported n-graphene layer films, Nano Lett. 6 (2006) 2667–2673.
[27] A.C. Ferrari, J.C. Meyer, V. Scardaci, C. Casiraghi, M. Lazzeri, F. Mauri, S. Piscanec, D. Jiang, K.S. Novoselov, S. Roth, A.K. Geim, Raman spectrum of graphene and graphene layers, Phys. Rev. Lett. 97 (2006) 187401.
[28] W.C. Oliver, G.M. Pharr, An improved technique for determining hardness and elastic modulus using load and displacement sensing indentation experiments, J. Mater. Res. 7 (1992) 1564–1583.
[29] Y.-G. Jung, B.R. Lawn, M. Martyniuk, H. Huang, X.Z. Hu, Evaluation of elastic modulus and hardness of thin films by nanoindentation, J. Mater. Res. 19 (2004) 3076–3080.
[30] X.Z. Hu, B.R. Lawn, A simple indentation stress–strain relation for contacts with spheres on bilayer structures, Thin Solid Films 322 (1998) 225–232.
[31] A.M. Al-Mayouf, A.A. Al-Swayih, N.A. Al-Mobarak, Effect of potential on the corrosion behaviour of a new titanium alloy for dental implant applications in fluoride media, Mater. Corros. 55 (2004) 88–94.
[32] P. Gilbert, J. Das, I. Foley, Biofilm susceptibility to antimicrobials, Adv. Dent. Res. 11 (1997) 160–167.

[33] O.G. Gold, H.V. Jordan, A selective medium for *Streptococcus mutans*, Arch. Oral. Res. 18 (1973) 1357–1364.
[34] B.G. Bibby, The use of fluorine in the prevention of dental caries. I. Rationale and approach, J. Am. Dent. Assoc. 31 (1944) 228–316.
[35] C.P. Dillon, Phorgotten phenomena: behavior of reactive metals, Mater. Perform. 7 (1998) 69–72.
[36] R. Strietzel, A. Hosch, In vitro corrosion of titanium, Biomater 19 (1998) 1495–1499.
[37] F. Mansfeld, Electrochemical methods of corrosion testing, ASM International ASM Handbook13A2003 446–462.
[38] G. Boere, Influence of fluoride on titanium in an acidic environment measured by the polarization resistance technique, J. Appl. Biomater. 6 (4) (1995) 283–288.
[39] M. Nakagawa, S. Matsuya, T. Shiraishi, M. Ohta, Effect of fluoride concentration and pH on corrosion behavior of titanium for dental use, J. Dent. Res. 78 (1999) 1568-72.
[40] R.W. Schutz, D.E. Thomas, Corrosion of titanium and titanium alloys, Metals handbook, 13, American Society for Metal (ASM) International, Metals Park, OH 1987, pp. 669–706.
[41] L. Kinani, A. Chtaini, Corrosion inhibition of titanium in artificial saliva containing fluoride, Leonardo J. Sci. 6 (11) (2007) 33–40.
[42] G. Ramírez, S.E. Rodil, S. Muhl, D. Turcio-Ortega, J.J. Olaya, M. Rivera, E. Camps, L. Escobar-Alarcón, Amorphous niobium oxide thin films, J. Non-Cryst. Solids 356 (50–51) (2010) 2714–2721.
[43] D. Zhu, H.-T. Lin, S. Mathur, T. Ohji, Aluminium Oxide and Silicon Nitride Thin Films as Anticorrosion Layers, Wiley-VCH, 2010.
[44] M. Marton, M. Vojs, E. Zdravecká, Raman spectroscopy of amorphous carbon prepared by pulsed arc discharge in various gas mixtures, J. Spectrosc. 2013 (2013) 1–6.
[45] Z.-K. Huang, K.-Sh. Chen, Nanoindentation fracture and fatigue characterisation of PECVD silicon nitride films subjected to rapid thermal annealing, Sensors Actuators A Phys. 207 (2014) 49–60.
[46] H. Huang, K.J. Winchester, A. Suvorova, R.R. Lawn, Y. Liu, Effect of deposition conditions on mechanical properties of low-temperature PECVD silicon nitride films, Mater. Sci. Eng. A 435–436 (2006) 453–459.
[47] P.-H. Wua, I.-K. Linc, H.-Y. Yana, K.-S. Oua, K.-S. Chena, X. Zhange, Mechanical property characterisation of sputtered and plasma enhanced chemical deposition (PECVD) silicon nitride films after rapid thermal annealing, Sensors Actuators A Phys. 168 (2011) 117–126.
[48] M. Vila, D. Ca'ceres, C. Prieto, Mechanical properties of sputtered silicon nitride thin films, J. Appl. Phys. 94 (2003) 7865–7873.
[49] D. Schneider, M.D. Tucker, Non-destructive characterization and evaluation of thin films by laser induced ultrasonic surface waves, Thin Solid Films 290–291 (1996) 305–311.
[50] O. Tabata, K. Kawahata, S. Sugiyama, I. Igarashi, Mechanical property measurements of thin films using load deflection of composite rectangular membranes, Sensors Actuators A: Phys. 20 (1989) 135–141.